Accepted Manuscript

Mechanism of formation of the honeycomb-like structures by the regime of the reversing current (RC) in the second range

Kata Berkesi, Predrag M. Živković, Nevenka Elezović, Uroš Lačnjevac, Evangelos Hristoforou, Nebojša D. Nikolić

Please cite this article as: Kata Berkesi, Predrag M. Živković, Nevenka Elezović, Uroš Lačnjevac, Evangelos Hristoforou, Nebojša D. Nikolić , Mechanism of formation of the honeycomb-like structures by the regime of the reversing current (RC) in the second range. Jeac (2018), https://doi.org/10.1016/j.jelechem.2018.12.021

Mechanism of formation of the honeycomb-like structures by
the regime of the reversing current (RC) in the second range

Kata Berkesi[1], Predrag M. Živković[2], Nevenka Elezović[3],
Uroš Lačnjevac[3], Evangelos Hristoforou[1], Nebojša D. Nikolić[4]

[1]National Technical University of Athens, School of Electrical and Computer Engineering,
Athens, Greece

[2] Faculty of Technology and Metallurgy, University of Belgrade, Karnegijeva 4, Belgrade, Serbia

[3]Institute of Multidisciplinary Research, University of Belgrade, Belgrade, Serbia

[4]ICTM-Department of Electrochemistry, University of Belgrade, Njegoševa 12, Belgrade, Serbia

Abstract. Electrodeposition of copper in the hydrogen co-deposition range by the regime of reversing current (RC) in the second range has been investigated by determination of the average current efficiency for hydrogen evolution reaction and by scanning electron (SEM) and optical (OM) microscopic analysis of the obtained deposits. Keeping the cathodic current density, the cathodic and the anodic pulses constant in all experiments, the anodic current density (j_a) values were varied: 40, 80, 160, 240 and 320 mA cm^{-2}. The Cu deposits produced by the RC regimes with different anodic current density values were compared with that obtained in a constant galvanostatic regime (DC) at the current density equal to the cathodic current density in the RC regimes. The honeycomb-like structures were formed in the DC regime and by the RC regimes with j_a of 40 and 80 mA cm^{-2}. The hole size in them was in the 60–70 μm range. Due to the decrease of quantity of evolved hydrogen with increasing anodic current density, the larger dish-like holes with dendrites at their bottom and shoulder were formed with j_a values of 160, 240 and 320 mA cm^{-2}. The maximum number of holes, and hence, the largest specific surface area of the honeycomb-like electrodes was obtained with $j_a = 80$ mA cm^{-2}, that can be ascribed to a suppression of coalescence of neighboring hydrogen bubbles. Application of the RC regime also led to the increase of uniformity of structures, what is concluded by cross section analysis of the formed honeycomb-like electrodes. For the first time, mechanism of Cu electrodeposition in the hydrogen co-deposition range by the RC regime in the second range was proposed and discussed.

1. Introduction

Formation of the honeycomb-like or 3D (three dimensional) foam structures by electrolysis represents a significant way for synthesis of open porous structures of the very high surface area [1–5]. Due to open porous structure, the 3D foam or the honeycomb-like structures are very suitable to be used as electrodes in many electrochemical devices, such as fuel cells, batteries and sensors, [1, 6, 7] as well as in catalytic purpose [8]. The open porous structure allows rapid transport of gas and liquid, while the extremely high surface area is desirable for electrochemical reactions. The main advantage of these 3D structures is determined by the orders of magnitudes higher specific surface area compared to the surface area of other one or two dimensional nano and micro structures. The method of formation of these structures by electrolysis is known as gas bubble dynamic template method or dynamic hydrogen bubble template (DHBT) method where hydrogen bubbles generated by electrodeposition at high overpotentials or current densities act as dynamic template around which metal electrodeposition occurs [3, 4, 6]. The main characteristics of these structures are macro-sized holes formed from detached hydrogen bubbles surrounded by nano porous cauliflower-like agglomerates of metal grains or dendrites formed around them [1, 2, 9]. The specific surface area of these structures is determined by number and size of holes, as well as by wall width among them [10]. Factors affecting the specific surface area are: regime of electrolysis, current density or overpotential applied for production, kind and composition of electrolyte, the type of working electrode, temperature of electrolysis, the addition of additives, etc. [3, 4].

There are a lot of studies on the formation of micro porous mono metal honeycomb-like structures with nano porous walls, like Cu [1, 2, 4, 9–14], Ag [15, 16], Au [17, 18], Pt [19], Pb [20], Sn [1], Ni [21–23], Pd [24] and Ru [25]. Some bimetallic systems have been performed with NiSn [26], NiCu [27, 28], NiCo [29], CuSn [6], CuPd [30], CuAu [31], CuAg [32], CuPt [33], CuFe [34], AuPt [35], PtPd [36], PdNi [37] and AgPd [38]. One research group published results on the production of the honeycomb-like NiCoFe ternary electrodes [39].

From all metals and alloys which can be obtained in the honeycomb-like form, copper is the most studied system [1, 2, 4, 9–14, 40–42]. The both galvanostatic [1, 10, 11] and potentiostatic [2, 4, 9, 14, 41, 42] regimes of electrolysis are widely used for production of Cu in the honeycomb-like form. The improvement of micro and nano structural characteristics of the Cu honeycomb-like electrodes can be achieved by addition of additives, such as acetic acid [10], chloride ions [10], $(NH_4)+$, polyethylene glycol and 3-mercapto-1-propane sulfonic acid [43]. In the last ten years, it was shown that the effects attained by use of additives on the increase of the specific surface area and the improvement of the structural stability of the honeycomb-like structures can be also achieved by application of periodically changing regimes of electrolysis in the millisecond range, such as pulsating overpotential (PO) [44–46], pulsating current (PC) [47–50] and reversing current (RC) [50, 51]. Some of advantages of application of periodically changing regimes of electrolysis in relation to the constant regimes of electrolysis are savings of chemicals because more electrolytes of different $CuSO_4$ and H_2SO_4 concentrations can be replaced by only one electrolyte by appropriate selection of parameters of square waves PO, PC and RC regimes, saving of place in the plating plants due to the reduced number of needed electrochemical cells, easier regulation of electrolyte composition due to avoidance of use of additives, prevention of contamination of electrolytes, etc [4]. The only limiting factor for commercial application of these regimes is considerably higher cost of pulse rectifier than conventional DC units [52]. However, pulse rectifiers using second range are simpler for construction, and hence cheaper for production, making them more suitable for production of the honeycomb-like structures than those working in the millisecond range. From all periodically changing regimes of electrolysis, the only RC regime is used in the second range [4]. For that reason, the aim of this study is formation of Cu honeycomb-like structures applying the reversing current (RC) regime in the second range with the special accent on mechanism of their formation.

2. Experimental

2.1. Electrochemical measurements

Electrodeposition of copper in the hydrogen co-deposition range was performed from 0.15 M $CuSO_4$ in 0.50 M H_2SO_4 in an open cell of cylindrical shape at the room temperature. Cu was electrodeposited galvanostatically at a current density of 320 mA cm^{-2} (DC mode) and by the

regime of reversing current (RC) in the second range. In all RC regimes, the cathodic current density, j_c of 320 mA cm^{-2}, a cathodic pulse, t_c of 10 s and an anodic pulse, t_a of 5 s were applied. The values of the anodic current density, j_a were: 40, 80, 160, 240 and 320 mA cm^{-2}. Electrodeposition of Cu was performed with a quantity of the electricity of 10 mA h cm^{-2}.

Doubly distilled water and analytical grade chemicals were used for the preparation of the solution for electrodeposition of copper. The working and counter electrodes were of pure Cu. The Cu working electrode was cylindrical shape of the overall surface area of 0.50 cm^2 (the length: 1.0 cm, diameter: 0.080 cm) situated in the middle of the cylindrical cell. The counter electrode was copper foil of 0.80 dm^2 surface area placed close to the walls of the cell.

2.2. The determination of the average current efficiency of hydrogen evolution ($\eta_{I,av}(H_2)$)

For the determination of the average current efficiency of hydrogen evolution, $\eta_{I,av}(H_2)$ an electrochemical cell with the same arrangement of copper electrodes as that used for the preparation of the copper deposits for SEM analysis was employed. The electrodes were situated under a burette with the surface facing up so that the total amount of hydrogen evolved during the electrodeposition processes went into the burette. In these measurements, the surface area of Cu working electrode situated under the burette was 0.63 cm^2. A drawing of the experimental setup for a measurement of volume of evolved hydrogen is presented in Fig. 1a. Before the beginning of the electrodeposition process ($t = 0$), an electrolyte in the burette was leveled up to upper line (Fig. 1b). When electrolysis is started, the electrolyte being suppressed by evolved hydrogen, and after certain time, t_i, it will reach some lower level, as schematically represented in Fig. 1b for $t = t_i$. The difference between the levels of electrolyte before the beginning of electrolysis and after certain time t_i represents a volume of evolved hydrogen $V(H_2)$ in a time t_i.

Then, the current efficiency of hydrogen evolution in a time t_i, $\eta_{I,i}(H_2)$, in %, is given by Eq. (1):

$$\eta_{I,i}(H_2) = \frac{V(H_2)}{\mu(H_2)S_0 j_c t_i} 100 \tag{1}$$

where

$$\mu(\mathrm{H}_2) = \frac{V}{nF} = \frac{24120\,\mathrm{cm}^3}{2 \times 26.8\mathrm{Ah}} = 450\frac{\mathrm{cm}^3}{\mathrm{Ah}} \tag{2}$$

and nF is the number of Faradays per mole of consumed ions, V is the molar volume of a gas at a temperature of 21.0 $^\circ$C (*i.e.* 24120 cm^3), S_0 is surface of working electrode, and j_c is the cathodic current density in the RC regimes, or the current density in the constant galvanostatic regime (DC mode).
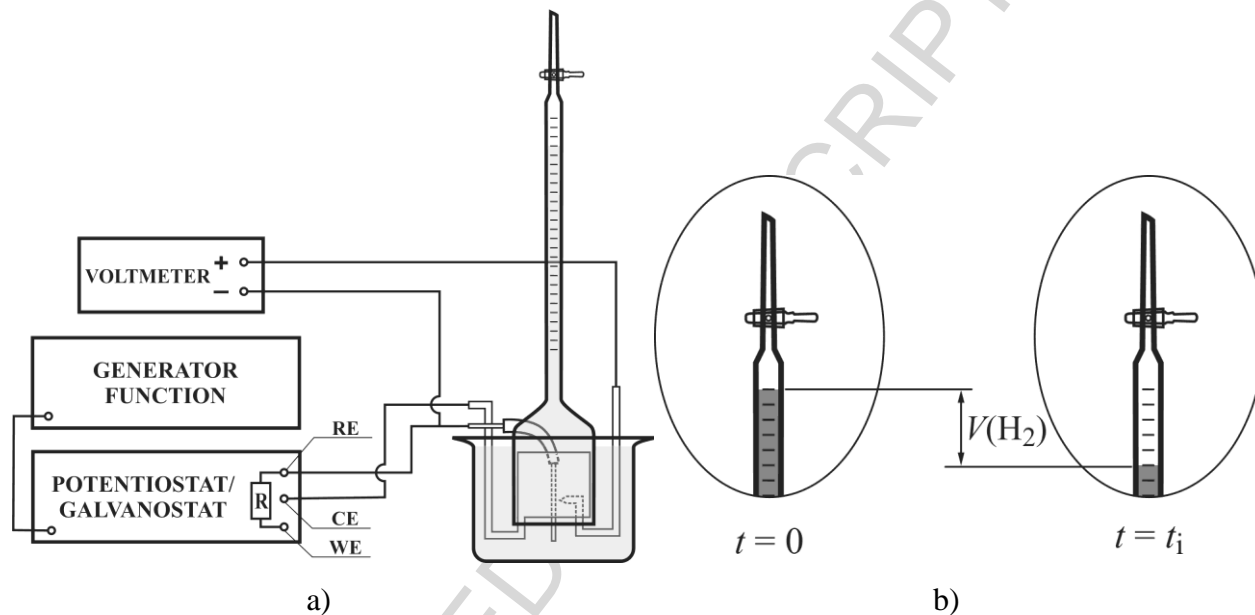

Figure 1. a) A drawing of the experimental setup for a measurement of volume of evolved hydrogen. WE – the working electrode; RE – the reference electrode; CE – the counter electrode, and b) schematic representation of hydrogen evolution for $t = 0$ and $t = t_i$.

The average current efficiency of hydrogen evolution, $\eta_{I,av}(\mathrm{H}_2)$ is determined after graphical integration $\eta_{I,i}(\mathrm{H}_2) - t$ as $\eta_{I,av}(\mathrm{H}_2) = (1/t)\int_0^t \eta_{I,i}(\mathrm{H}_2)\mathrm{d}t$.

Alternatively, for the DC mode, the current efficiency for hydrogen evolution reaction, η_{I,H_2} can be determined by a measurement of amount of electrodeposited Cu using Eq. (3) [22]:

$$\eta_{I,\mathrm{H}_2} = \left(1 - \frac{mnF}{jS_0 M(\mathrm{Cu})t}\right) \cdot 100 \tag{3}$$

where m is mass of electrodeposited Cu, j is a current density applied in the DC mode, t is time, and $M(Cu)$ is molar mass of copper.

Due to a dissolution effect during anodic pulses, this alternative method is no suitable for determination of the current efficiency for hydrogen evolution reaction for the RC regime in the second range.

2.3. Characterization of the produced deposits

Morphologies of Cu deposits obtained by DC regime and the RC regimes in the second range with various j_a values were characterized by the technique of scanning electron microscopy (SEM) using TESCAN Digital Microscopy - model VEGA3, Brno, Czech Republic.

Cross section analysis was performed using optical microscope (Olympus CX41) connected to the computer. Preparation of the samples for cross section analysis is described elsewhere [51].

3. Results and discussion

3.1. The determination of the average current efficiency for hydrogen evolution reaction

The regime of reversing current (RC) is defined by Eq. (4) [4]:

$$j_{av} = \frac{j_c t_c - j_a t_a}{t_c + t_a} \tag{4}$$

where j_{av} is the average current density, j_c is the cathodic current density, j_a is the anodic current density, t_c is the cathodic time, and t_a is the anodic time.

Since

$$r = \frac{t_a}{t_c} \tag{5}$$

Eq. (4) can be written in the form:

$$j_{av} = \frac{j_c - j_a r}{1 + r} \tag{6}$$

In the hydrogen co-deposition range, parallel to metal electrodeposition hydrogen evolution occurs, and the current efficiency for metal electrodeposition (in our case copper) is less than 1. In this case, the average current density can be presented by Eq. (7):

$$j_{av}* = \frac{\eta_{I,c}(Cu) j_c - j_a r}{1 + r} \tag{7}$$

where $j_{av}*$ is the average current density in the conditions of hydrogen evolution at the cathode, and $\eta_{I,c}(Cu)$ is the current efficiency for Cu electrodeposition during the cathodic pulses, since there is no any gas evolution during anodic times [51]. Eq. (7) can be re-written in the form:

$$j_{av}* = \frac{[1 - \eta_I(H_2)] j_c - j_a r}{1 + r} \tag{8}$$

since

$$\eta_{I,c}(Cu) + \eta_I(H_2) = 1 \tag{9}$$

The average current efficiency for hydrogen evolution, $\eta_{I,av}(H_2)$ is determined from the dependencies of the volume of hydrogen evolved during electrodeposition process on time of electrodeposition according to procedure described in Experimental. Figure 2 shows the dependencies of volume of evolved hydrogen, $V(H_2)$ and the current efficiency of hydrogen evolution, $\eta_{I,i}(H_2)$ on time of electrodeposition obtained at a current density of 320 mA cm^{-2}, and by the RC regimes with j_a of 40 and 80 mA cm^{-2} (Fig. 2a) and with j_a of 160, 240 and 320 mA cm^{-2} (Fig. 2b). The values of the average current efficiency of hydrogen evolution determined as $\eta_{I,av}(H_2) = (1/t) \int_0^t \eta_{I,i}(H_2) dt$ are given in Table 1. The decrease of both the volume of evolved hydrogen and the average current efficiency of hydrogen evolution with increasing the anodic current density was observed by the application of the RC regimes in the second range.
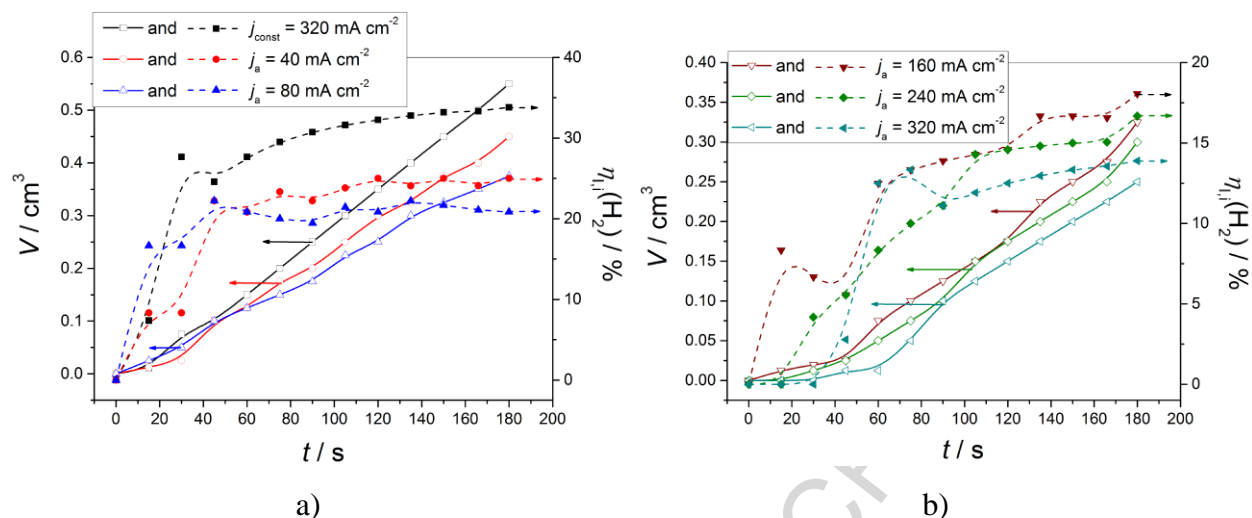
Figure 2. The dependencies of the volume of evolved hydrogen and the current efficiency of hydrogen evolution on the time of electrodeposition obtained at: a) a constant current density of 320 mA cm^{-2} (DC mode), and by the RC regimes with j_a of 40 and 80 mA cm^{-2}, and b) with j_a of 160, 240 and 320 mA cm^{-2}.

Table 1. The values of the average current efficiency for hydrogen evolution reaction obtained in the constant galvanostatic (DC) mode at $j = 320$ mA cm^{-2}, and in the RC regimes with the values of j_a of 40, 80, 160, 240 and 320 mA cm^{-2}.

j_a / mA cm^{-2}	DC regime	40	80	160	240	320
$\eta_{I,av}(H_2)$ / %	32.8	26.6	20.5	18.0	15.1	12.8

The value of the current efficiency of hydrogen evolution determined by a measurement of amount of electrodeposited Cu in the DC mode at a current density of 320 mA cm^{-2} was 32.5 %. The excellent agreement between the values obtained on these two ways was observed.

3.2. Morphological and structural analysis of Cu deposits obtained by the galvanostatic and reversing current (RC) in the second range regimes

Morphologies of Cu deposits obtained at a constant current density (DC mode) of 320 mA cm^{-2} and by the reversing current (RC) regimes in the second range with the anodic current

densities (j_a) of 40, 80, 160, 240 and 320 mA cm^{-2} are shown in Fig. 3. In all RC regimes, the cathodic current density of 320 mA cm^{-2}, a cathodic pulse of 10 s and an anodic pulse of 5 s were applied. The durations of cathodic and anodic pulses were selected to be inside range for which this regime in the second range should give optimal results [4]:

$$1.5 \leq t_c/t_a \leq 5 \tag{10}$$

or

$$3 \text{ s} \leq t_c + t_a \leq 16 \text{ s} \tag{11}$$
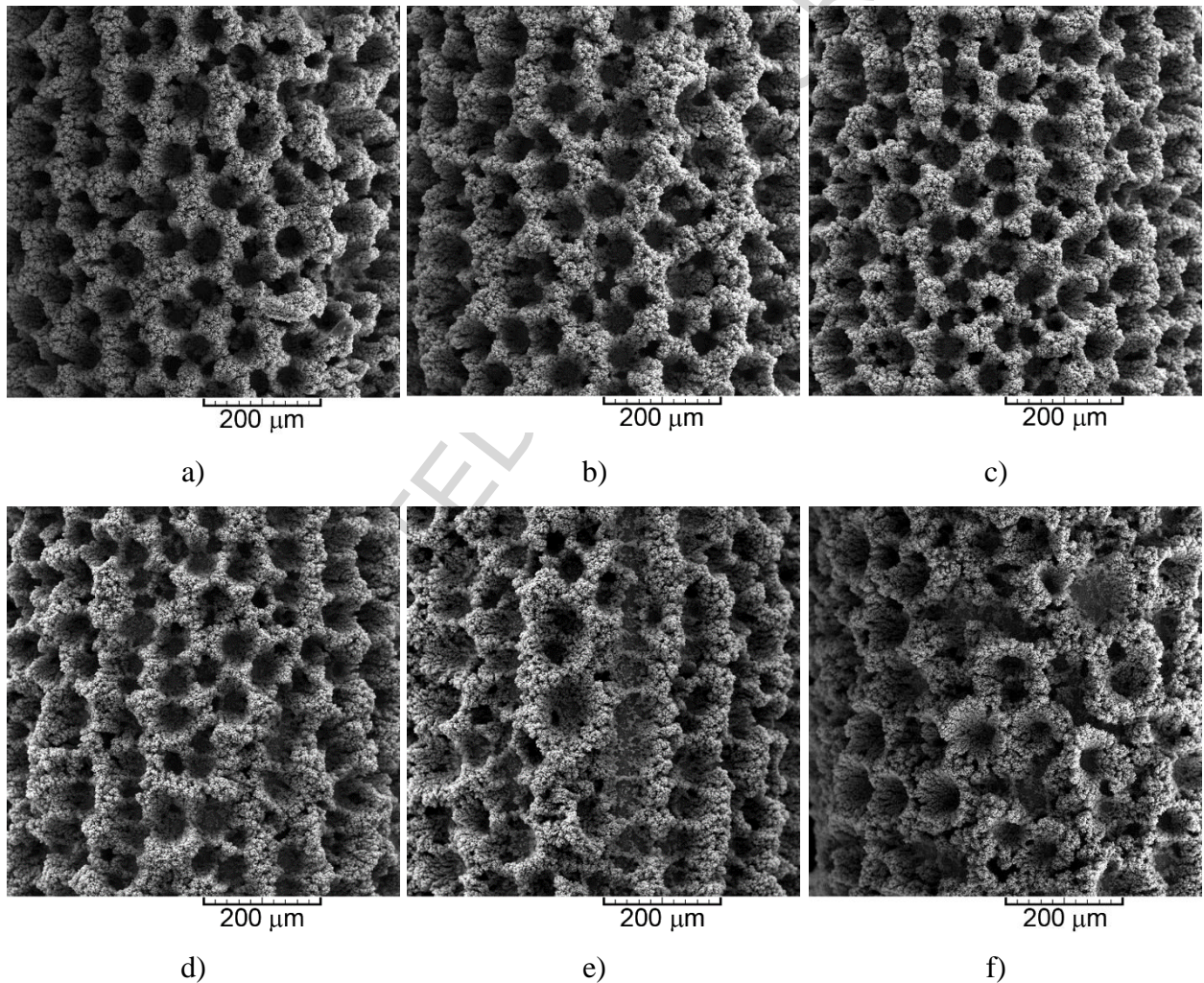

Figure 3. Morphologies of Cu deposits obtained by electrodeposition at: a) constant current density of 320 mA cm^{-2} (DC mode), and by the RC regimes with j_a of: b) 40, c) 80, d) 160, e) 240 and f) 320 mA cm^{-2}.

The dominant presence of holes formed from the detached hydrogen bubbles as consequence of vigorous hydrogen evolution reaction under these electrodeposition conditions was characteristic of all shown structures. However, their careful analysis showed a certain differences among them, indicating the strong effect of the applied anodic current density values not only on the amount of evolved hydrogen, but to also on the shape, size and distribution of the holes.

The uniform honeycomb-like structures are formed in the DC mode and by the RC regimes with j_a of 40 and 80 mA cm^{-2} (Fig. 3a–c). The typical holes constructing the honeycomb-like structure, denoted as "non-coalesced" type of holes [4], obtained in the DC mode and with j_a of 80 mA cm^{-2} are shown in Fig. 4a and b, respectively. The size of these holes was in the range 60–70 μm, without any difference among those obtained in the DC mode and those obtained with j_a of 40 and 80 mA cm^{-2}. Aside from this type of holes, the presence of holes obtained by a coalescence of neighboring hydrogen bubbles was mentioned in the Cu structures obtained in the DC mode and with j_a of 40 mA cm^{-2}. Formation of these holes is a consequence of more vigorous hydrogen evolution at a current density of 320 mA cm^{-2} and with j_a of 40 mA cm^{-2} than with j_a of 80 mA cm^{-2}. This type of holes is denoted as "coalesced" type [4], and the typical representative of this type obtained with j_a of 40 mA cm^{-2} is shown in Fig. 4c. The diameter of these holes was about 100 μm. The third type of holes is formed with j_a of 160, 240 and 320 mA cm^{-2}. The typical hole from this group obtained with j_a of 320 mA cm^{-2} is shown in Fig. 4d. This type of holes has conspicuous edges classifying them into the group of the dish-like holes [4, 40]. The size of these holes was larger than 100 μm. Small dendrites were formed at their shoulders (Fig. 4e). Formation of these holes is a consequence of further decrease of the amount of evolved hydrogen with the applied anodic current densities of 160, 240 and 320 mA cm^{-2} (Table 1).
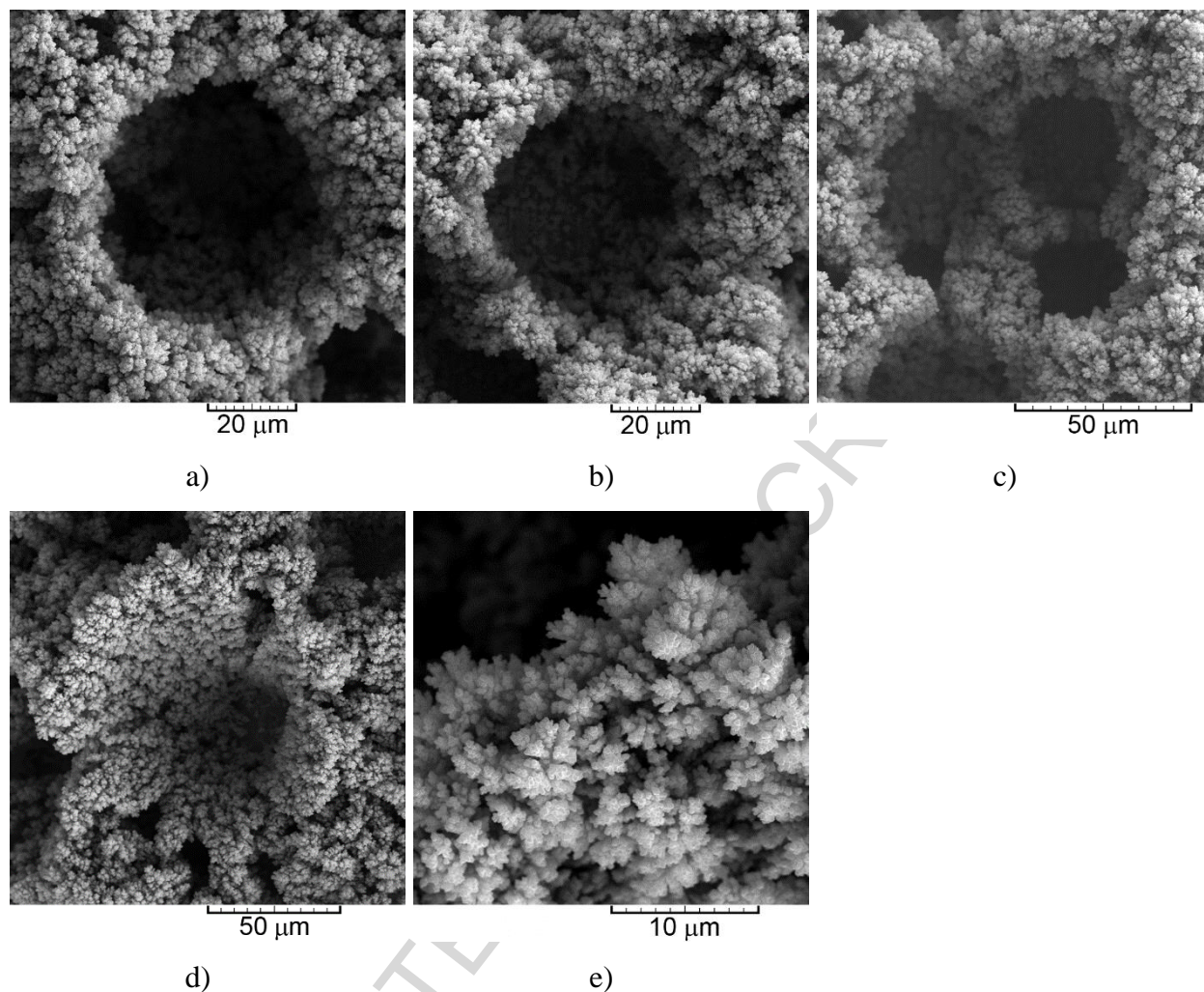
Figure 4. The typical holes formed from the detached hydrogen bubbles: "non-coalesced" type of holes obtained in: a) the DC mode and b) the RC with j_a of 80 mA cm^{-2}, c) "coalesced" type of hole obtained with j_a of 40 mA cm^{-2}, and d) and e) dish-like hole obtained with j_a of 320 mA cm^{-2}.

The dependence of the number of holes on the applied anodic current density values is shown in Fig. 5. For the honeycomb-like structure obtained in the DC mode, the value j_a of 0 mA cm^{-2} is taken. The increase of the number of holes with the applied j_a values of 40 and 80 mA cm^{-2} in relation to the DC regime can be primarily ascribed to suppressed coalescence of neighboring hydrogen bubbles. The decrease after reached maximum with j_a of 80 mA cm^{-2} is a consequence of a decrease of the amount of evolved hydrogen with increasing the anodic current density values accompanied by formation of the larger dish-like holes.
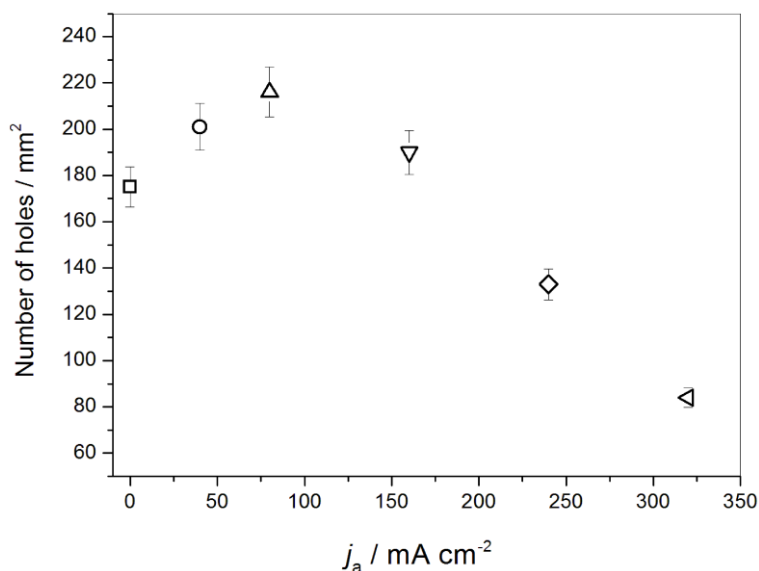
Figure 5. The dependence of the number of holes on the applied anodic current density values. For the honeycomb-like structure obtained in the DC mode, the value j_a of 0 mA cm^{-2} is taken.

Aside from on the shape and size of holes, the applied anodic current densities also had the strong effect on appearance of the bottom of holes. In the dependence of j_a values, the two types of bottom were formed. The first type corresponds to the bottom of so-called "coalesced hole" and "non-coalesced" holes (the holes obtained in the DC mode and with j_a values of 40 and 80 mA cm^{-2}). The bottom of these holes is relatively compact and constructed from small cauliflower-like agglomerates of Cu grains, as presented in Fig. 6a showing the bottom of the hole obtained in the DC regime. The second type corresponds to the bottom of holes obtained with j_a of 160, 240 and 320 mA cm^{-2}. The very branchy 3D (three dimensional) dendrites, like those presented in Fig. 6b and c showing the bottom of the hole obtained with j_a of 160 mA cm^{-2}, were formed at the bottoms of these holes.
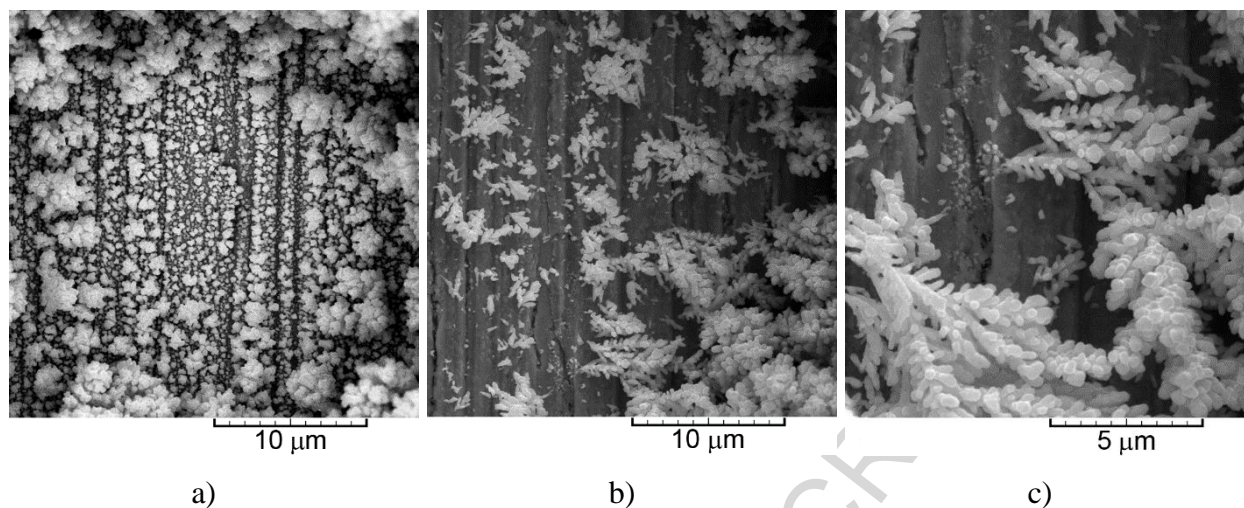
Figure 6. The types of bottom of formed holes: a) compact bottom constructed from small cauliflower-like agglomerates of Cu grains obtained in the DC mode, and b) and c) the bottom constructed from the very branchy dendrites obtained with j_a of 160 mA cm^{-2}.

Figure 7 shows cauliflower-like agglomerates of Cu grains formed among holes obtained with j_a of 80 mA cm^{-2} (Fig. 7a) and with j_a of 160 mA cm^{-2} (Fig. 7b). The very disperse cauliflower-like agglomerates of Cu grains were formed with both j_a values. These agglomerates were mutually separated by irregular channels which origin is a consequence of strong hydrogen evolution. It is necessary to note that the small dendrites were formed at the tops of cauliflower-like agglomerates formed with j_a of 160 mA cm^{-2} (Fig. 7b). The cauliflower-like agglomerates of Cu grains obtained with j_a of 80 mA cm^{-2} were very similar to those obtained in the DC mode and with j_a of 40 mA cm^{-2}. On the other hand, the cauliflower-like agglomerates of Cu grains obtained with j_a of 160 mA cm^{-2} were similar to those obtained with j_a of 240 and 320 mA cm^{-2}. The average distances among holes (so-called the wall width) in the honeycomb-like structures were: 32 µm for the honeycomb-like structure obtained in the DC mode, and 29 µm and 25 µm for those obtained with j_a values of 40 and 80 mA cm^{-2}, respectively. The further increase of j_a values above 80 mA cm^{-2} led to the decrease of number of the holes (Fig. 5), and consequently, up to the noticeable increase of distances among them.
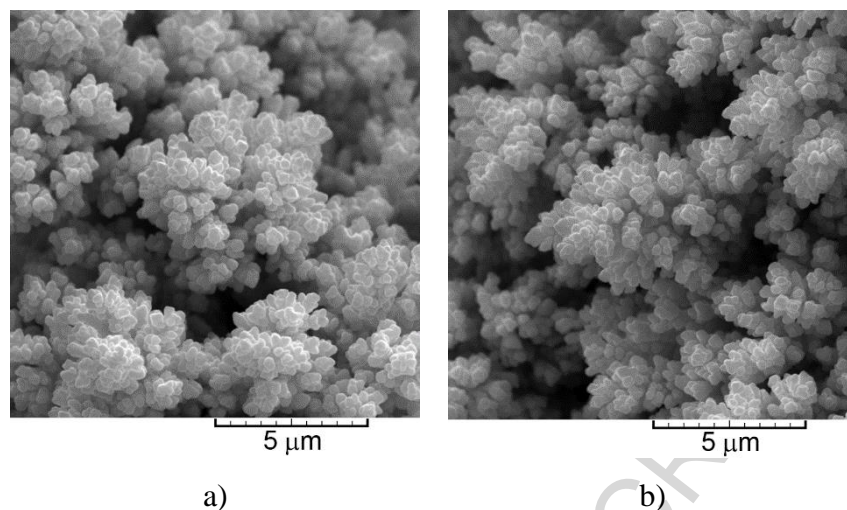
Figure 7. The cauliflower-like agglomerates of Cu grains formed among holes by the RC regimes with j_a of: a) 80, and b) 160 mA cm^{-2}.

The completed insight in structure of the deposits obtained in the DC mode and with various anodic current densities is obtained by their cross section analysis. The holes originating from detached hydrogen bubbles in the honeycomb-like structure obtained in the DC mode are shown in Fig. 8a and b. The diameter of holes is in good agreement with those observed by the SEM analysis. The depth of holes is about 100 μm. Application of the RC regimes with j_a of 40 and 80 mA cm^{-2} did not affect the depth of holes, as shown in Fig. 8c and d, respectively. The presence of "coalesced" holes in the honeycomb-like structures obtained in the DC mode and with j_a of 40 mA cm^{-2} is also identified (Fig. 8e; the hole obtained in the DC mode). Cross section of the dish-like hole obtained with j_a of 320 mA cm^{-2} is shown in Fig. 8f. All differences of this type of holes in relation to the other types of holes like conspicuous edges, dendrites at the bottom and larger diameter are clearly seen from Fig. 8f. The increased uniformity of the honeycomb-like structures attained by application of the RC regimes with j_a of 40 and 80 mA cm^{-2} in relation to the one obtained in the DC mode can be easily seen by cross section analysis of the structures obtained under these electrodeposition conditions (Fig. 8a, c and d). Finally, the typical nanoporous structure formed through the interiour of the honeycomb-like structure produced with j_a of 80 mA cm^{-2} is shown in Fig. 8g. Numerous pores are interconnected making a channel structure through the interior of the deposit.
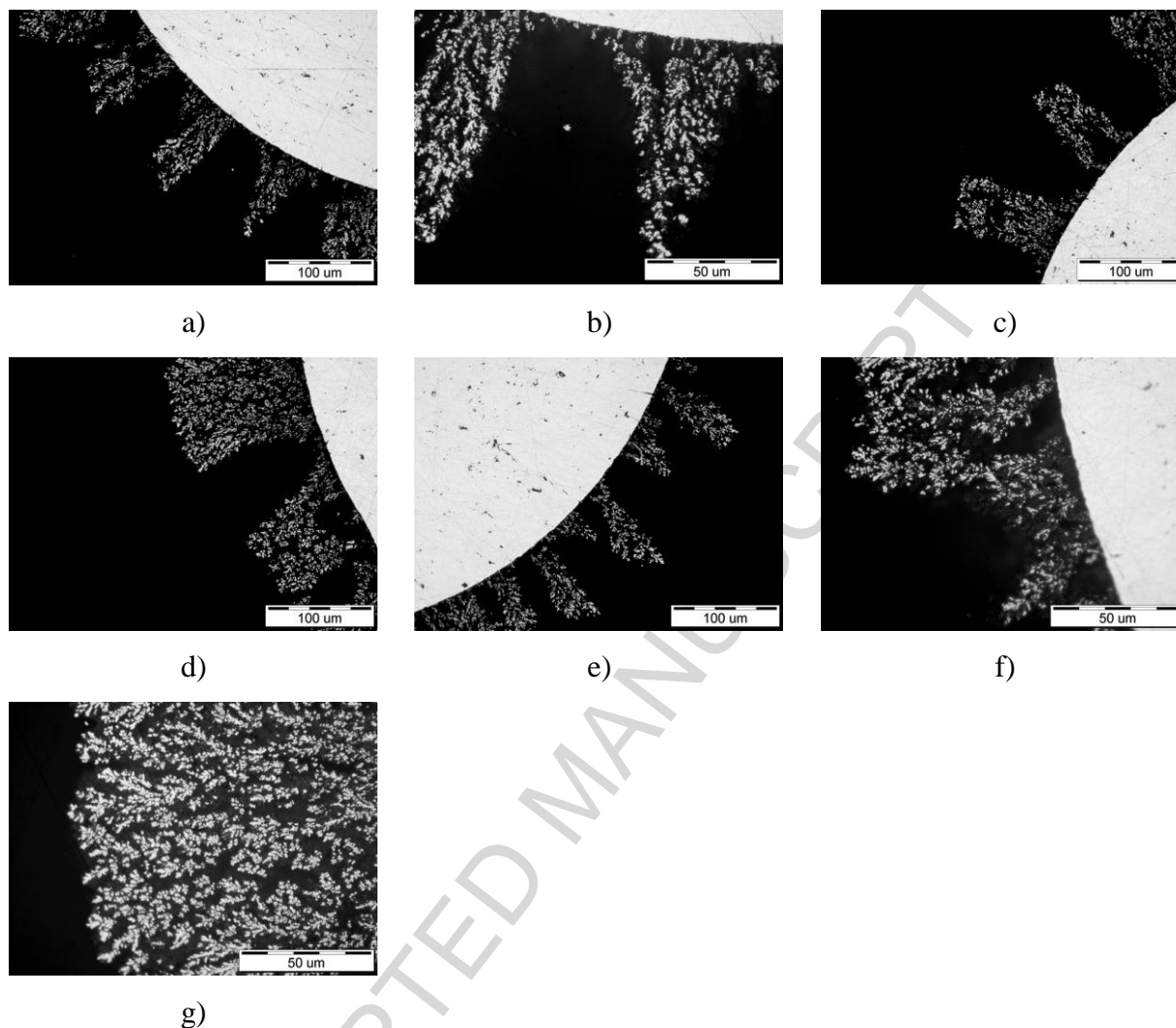
Figure 8. Cross sections of the structures obtained in the DC mode and by the RC regimes with different j_a values: a) and b) the DC mode, c) 40 mA cm^{-2}, d) 80 mA cm^{-2}, e) the DC mode, f) 320 mA cm^{-2}, and g) 80 mA cm^{-2}.

3.3. Discussion of presented results

On the basis of the presented morphological and structural analysis of Cu deposits, it is clear that all deposits can be classified into two groups. In the first group are situated the honeycomb-like structures characterized by uniform distribution of holes and cauliflower-like agglomerates of Cu grains among them. They were obtained in the DC regime and the RC regimes with j_a of 40 and 80 mA cm^{-2}, and their formation was accompanied by $\eta_{I,av}(H_2)$ in the

range 20.5–32.8 %. In the second group are situated Cu deposits obtained with j_a of 160, 240 and 320 mA cm^{-2}. The amounts of evolved hydrogen spent for their formation (see $\eta_{I,av}(H_2)$ in Table 1) were smaller than those spent for formation of the honeycomb-like structures. As a result of this decrease, the strong morphological and structural changes in the deposits were observed. The decrease of number of holes, the appearance of dish-like holes with dendrites at their shoulders, as well as very branchy 3D dendrites formed at the bottom of holes were a consequence of an application of the j_a values of 160, 240 and 320 mA cm^{-2}.

Anyway, all shown deposits are formed in conditions of cosiderable hydrogen evolution as the parallel reaction to Cu electrodeposition. The uniform distribution of holes and cauliflower-like agglomerates of Cu grains among them in the honeycomb-like structures clearly indicate vigorous evolution of hydrogen making the strong effect on the hydrodynamic conditions in the near-electrode layer. Vigorous hydrogen evolution causes a stirring electrolyte in the near-electrode layer leading to a decrease of the thickness of the diffusion layer, an increase in the limiting diffusion current density, and a decrease in the degree of diffusion control of the electrodeposition process [2, 4]. The concept of "effective overpotential" originally proposed to explain formation of the honeycomb-like structures in the potentiostatic regime [2], and later extended to involve periodically changing current regimes in the millisecond range (the PC and the RC regimes) [48, 51] can be also applied for the RC regime in the second range. According to this concept, when hydrogen evolution is enough vigorous, electrodeposition process occurs at overpotential or potential which is effectively lower than that specified, and this overpotential or potential is denoted as "effective" in a deposition process. From the morphological point of view, this means that the morphologies of metal deposits become similar to those obtained at some lower overpotentials at which hydrogen evolution does not occur or is very slow. The absence of dendrites in the honeycomb-like structures obtained in the DC mode, and with j_a of 40 and 80 mA cm^{-2} clearly confirms correctness of application of this concept here. The effectiveness of stirring of electrolyte by evolved hydrogen was considerably decreased with j_a larger than 80 mA cm^{-2} causing a non-uniformity of the surfaces formed with j_a of 160, 240 and 320 mA cm^{-2}. As result of this decrease of effectiveness of solution stirring, the decrease of number of holes, the appearance of dish-like holes and dendrites was observed.

Mechanism of electrodeposition in the hydrogen co-deposition range by application of periodically changing regimes of electrolysis in the millisecond range, such as PO [44–46], PC [47–50] and RC [50, 51], has been well investigated and elaborated in the literature [4]. The common characteristic of all these regimes is that electrodeposition processes in the millisecond range occur at the average current densities which were attained by selection of parameters of the square-wave regimes. As for as electrodeposition processes in the hydrogen co-deposition range by the RC regime in the second range, mechanism is completely different, that can be considered as follows: in the initial stage of electrodeposition by the RC regime in the second range, during the first cathodic pulse of 10 s electrodeposition process occurs as in the constant galvanostatic regime. The selected value j_c of 320 mA cm^{-2} belongs to the hydrogen co-deposition range with a cathodic potential (E_c) response of 1150–1250 mV. As a result of this, the approximately same number of hydrogen bubbles is formed in the initial stage of the electrodeposition irrespective of the applied j_a value. During anodic pulses of 5 s, dissolution process occurs with the selected anodic current density and the corresponding anodic potential (E_a) responses are just function of applied j_a value. The larger j_a value, the larger E_a response is observed. The ranges of anodic potentials during the first anodic pulse obtained at the examined j_a values are given in Table 2. In the next cathodic pulse, the initial cathodic potential corresponds to the final anodic potential reaching the value corresponding to the hydrogen co-deposition range (1150–1250 mV) after a certain time, $t_{c,est}$. With increasing the j_a values, it prolongs a time needed to reach this E_c response. The $t_{c,est}$ values needed to reach E_c response during the cathodic pulses are also given in Table 2. In this way, it decreases an effective time, $t_{c,eff}$ for electrodeposition in the hydrogen co-deposition range which is responsible for formation of the honeycomb-like structures, because it is valid $t_{c,est} + t_{c,eff} = t_c$, or $t_{c,est} + t_{c,eff} = 10$ s in our case. For easier understanding, Fig. 9 shows the schematic illustration of the constant galvanostatic regime (Fig. 9a) and the two square wave RC regimes like those obtained with j_a of 80 (Fig. 9b) and 320 mA cm^{-2} (Fig. 9c).
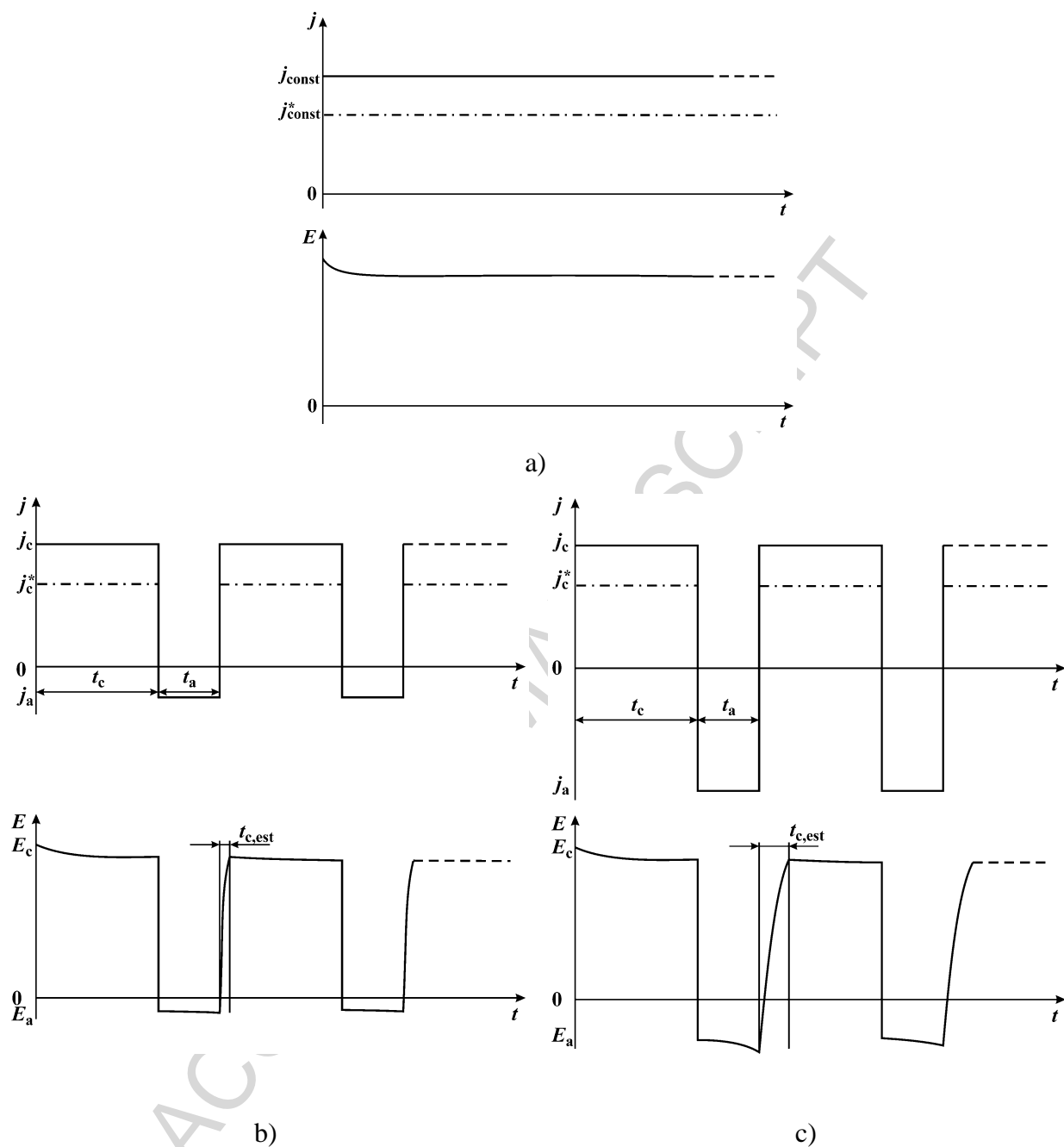
Figure 9. The schematic illustrations of: a) the constant galvanostatic regime, and the square wave RC regimes in the second range like those observed with: b) $j_a = 80$ mA cm^{-2} and c) $j_a = 320$ mA cm^{-2}.

Table 2. The anodic current density (j_a), the $t_{c,est}$ time needed to reach cathodic potential corresponding to the hydrogen co-deposition range and the range of anodic potentials (ΔE_a) during the first anodic pulse.

j_a / mA cm^{-2}	40	80	160	240	320
ΔE_a / mV	48–75	108–122	174–212	242–312	320–420
$t_{c,est}$ / s	0.40	0.82	1.40	1.96	2.42

From this consideration, it is clear that there is a critical j_a value enabling formation of the honeycomb-like structures. For the conditions presented here, the critical value giving the maximum number of holes corresponds to j_a of 80 mA cm^{-2}. Above this value, dissolution process becomes too strong and $t_{c,eff}$ is not enough long to keep formation of the honeycomb-like structures. Due to a shortening of $t_{c,eff}$, it decreases the amount of hydrogen produced during cathodic pulses, and as result of this, some of initially formed hydrogen bubbles detach from the electrode surface before they are developed in the large bubbles (or holes). In this way, the number of holes formed from the detached hydrogen bubbles decreases with the increase of j_a value. The second consequence of decreased amount of generated hydrogen is the appearance of dendrites.

The complete insight of applied RC regimes in the second range on morphology of Cu deposits cannot be obtained without a consideration of the current density distribution effect. Namely, during anodic pulses, the current lines are primarily concentrated at the higher points (or the tips) of growing surfaces due to the edge effect [4], causing their faster dissolution than the other parts of the surface. As result of this selective dissolution of copper, the increased uniformity of the honeycomb-like structures obtained with the j_a of 40 and 80 mA cm^{-2} was observed in relation to the DC mode (Fig. 8a, c and d). The dissolved Cu ions being removed from the diffusion layer by convection created by the movement of detached hydrogen bubbles produced during cathodic pulse ("current of hydrogen"). As a result of successful removal of Cu ions from the diffusion layer, the composition of the electrolyte near to the electrode surface is similar to that before previous cathodic pulse [33]. This is a macro effect on morphology of the growing structures. Simultaneously, the particles with lower tip radii are dissolved faster than those with larger ones [53] (micro effect on morphology of the structure). The effect of the

anodic current density grows with the further increase of the j_a values leading to a formation of very non-uniform electrode surfaces.

The following advantages in formation of the honeycomb-like structures by application of the RC regime in the second range in relation to those produced in the constant galvanostatic regime were attained: (a) the increase of the specific surface area of the honeycomb-like electrodes manifested by the increase of the number of holes due to a suppression of coalsescence of neighboring hydrogen bubbles and by the decrease of distances among them (the wall width), and (b) the improvement of the structural stability due to the decrease of the amount of evolved hydrogen spent for their formation. The number of holes formed by the RC regime with j_a of 80 mA cm^{-2} was about 20 % larger than the number of holes formed in the DC regime. On the other hand, the $\eta_{I,av}(H_2)$ value obtained for the RC regime with j_a of 80 mA cm^{-2} (the maximum specific surface area) was about 37.5 % smaller than the one obtained for the honeycomb-like structure produced in the DC mode at the current density equal to the cathodic current density in the RC regime. As already mentioned, the only current limiting factor for technological application of the RC regime in the second range on formation of the honeycomb-like structures is still higher cost of a pulse rectifier than a DC unit [52]. It is a highly regulated and sophisticated design that costs more to manufacture. However, the fast development of electronic industry will probably decrease a cost of these rectifiers and will enable their larger commercial application.

4. Conclusions

The processes of copper electrodeposition in the hydrogen co-deposition range by the regime of reversing current (RC) in the second range have been examined. The quantities of evolved hydrogen were quantified by the determination of the average current efficiencies for hydrogen evolution reaction, while the techniques of scanning electron (SEM) and optical (OM) microscopy were used for morphological and structural analysis of the formed deposits, respectively. In all RC experiments, the values of the cathodic current density (j_c) and the cathodic (t_c) and the anodic (t_a) times are kept constant ($j_c = 320$ mA cm^{-2}; $t_c = 10$ s; $t_a = 5$ s), while the following anodic current density (j_a) values were analyzed: 40, 80, 160, 240 and 320

mA cm^{-2}. The deposits obtained by different RC regimes were compared with the one obtained by the constant galvanostatic regime (DC) at the current density equal to the cathodic current density in the RC experiments (320 mA cm^{-2}). Following these electrodeposition conditions, it was shown:

(a) the uniform honeycomb-like structures were formed in the DC regime and by the RC regimes with j_a of 40 and 80 mA cm^{-2},

(b) the hole size in the honeycomb-like structures was in the 60–70 μm range. Holes obtained by coalescence of closely formed hydrogen bubbles were found in the honeycomb-like structures obtained in the DC mode and by the RC regime with j_a of 40 mA cm^{-2}. The dish-like holes sizes of about 100 μm were formed with j_a of 160, 240 and 320 mA cm^{-2}.

(c) The very branchy 3D dendrites were formed at the bottom and shoulder of the dish-like holes as a result of the decrease of quantity of evolved hydrogen with increasing the anodic current density.

As a consequence of suppression of coalescence of closely formed hydrogen bubbles, the maximum specific surface area of the honeycomb-like structures, determined by the number and size of holes formed from the detached hydrogen bubbles, was obtained with j_a of 80 mA cm^{-2}. The improvement of morphological and structural characteristics of the honeycomb-like structures obtained by the appropriate RC regimes relative to those obtained by the DC regime was observed.

For the first time, mechanism of copper electrodeposition in the hydrogen co-deposition range by the RC regime in the second range has been considered.

References

[1] H.C. Shin, J. Dong, M. Liu, Nanoporous Structures Prepared by an Electrochemical Deposition Process, *Adv Mater* **15** (2003) 1610–1614. doi:10.1002/adma.200305160

[2] N.D. Nikolić, K.I. Popov, Lj.J. Pavlović, M.G. Pavlović, The effect of hydrogen codeposition on the morphology of copper electrodeposits. I. The concept of effective overpotential, *J Electroanal Chem* **588** (2006) 88–98. doi:10.1016/j.jelechem.2005.12.006

[3] B.J. Plowman, L.A. Jones, S.K. Bhargava, Building with bubbles: the formation of high surface area honeycomb-like films via hydrogen bubble templated electrodeposition, *Chem Commun* **51** (2015) 4331–4346. doi: 10.1039/c4cc06638c

[4] K.I. Popov, S.S. Djokić, N.D. Nikolić, V.D. Jović, Morphology of Electrochemically and Chemically Deposited Metals, Springer: New York, USA, 2016, pp. 1–368.

[5] M. Wang, X.Yu, Z.Wang, Z. Guo, L. Dai, Hierarchically 3D porous films electrochemically constructed on gas-liquid-solid three-phase interface for energy application, *J Materials Chem A* **5** (2017) 9488–9513. doi: 10.1039/c7ta02519j

[6] H.C. Shin, M. Liu, Three-dimensional porous copper-tin alloy electrodes for rechargeable lithium batteries, *Adv Funct Mater* **15** (2005) 582–586. doi: 10.1002/adfm.200305165

[7] R. Kim, D. Han, D. Nam, J. Kim, H. Kwon, Effects of Substrate Morphology and Post electrodeposition on Structure of Cu Foam and Their Application for Li-Ion Batteries, *J Electrochem Soc* **157** (2010) D269–D273. doi: 10.1149/1.3356974

[8] J. Yin, J. Jia, L. Zhu, Macroporous Pt modified glassy carbon electrode: Preparation and electrocatalytic activity for methanol oxidation, *Int J Hydrogen Energy* **33** (2008) 7444–7447. doi:10.1016/j.ijhydene.2008.10.019

[9] N.D. Nikolić, K.I. Popov, Hydrogen Co-deposition Effects on the Structure of Electrodeposited Copper. In: S.S. Djokić (Ed) Electrodeposition: Theory and Practice. Series: Modern Aspects of Electrochemistry, vol 48. Springer, New York, 2010, pp 1–70.

[10] H.C. Shin, M. Liu, Copper foam structures with highly porous nanostructured walls, *Chem Mater* **16** (2004) 5460–5464. doi: 10.1021/cm048887b

[11] Y. Li, W.-Z. Jia, Y.-Y. Song, X.-H. Xia, Superhydrophobicity of 3D porous copper films prepared using the hydrogen bubble dynamic template, *Chem Mater* **19** (2007) 5758–5764. doi: 10.1021/cm071738j

[12] N.D. Nikolić, G. Branković, M.G. Pavlović, K.I. Popov, The effect of hydrogen codeposition on the morphology of copper electrodeposits. II. Correlation between the properties of

electrolytic solutions and the quantity of evolved hydrogen, *J Electroanal Chem* **621** (2008) 13–21. doi:10.1016/j.jelechem.2005.12.006

[13] W. Zhang, C. Ding, A. Wang, Y. Zeng, 3-D Network Pore Structures in Copper Foams by Electrodeposition and Hydrogen Bubble Templating Mechanism, *J Electrochem Soc* **162** (2015) D365-D370. doi: 10.1149/2.0591508jes

[14] H. Singh, P.B. Dheeraj, Y.P. Singh, G. Rathore, M. Bhardwaj, Electrodeposition of porous copper as a substrate for electrocatalytic material, *J Electroanal Chem* **785** (2017) 1–7. doi: 10.1016/j.jelechem.2016.12.013

[15] S. Cherevko, X. Xing, C.-H. Chung, Electrodeposition of three-dimensional porous silver foams, *Electrochem Commun* **12** (2010) 467–470. doi:10.1016/j.elecom.2010.01.021

[16] S. Cherevko, C.-H.Chung, Impact of key deposition parameters on the morphology of silver foams prepared by dynamic hydrogen template deposition, *Electrochim Acta* **55** (2010) 6383–6390. doi: 10.1016/j.electacta.2010.06.054

[17] B.J. Plowman, A.P. O'Mullane, P.R. Selvakannan, S.K. Bhargava, Honeycomb nanogold networks with highly active sites, *Chem Commun* **46** (2010) 9182–9184. doi:10.1039/c0cc03696j

[18] S. Cherevko, C.-H. Chung, Direct electrodeposition of nanoporous gold with controlled multimodal pore size distribution, *Electrochem Commun* **13** (2011) 16–19. doi:10.1016/j.elecom.2010.11.001

[19] A. Ott, L.A. Jones, S.K. Bhargava, Direct electrodeposition of porous platinum honeycomb structures, *Electrochem Commun* **13** (2011) 1248–1251. doi: 10.1016/j.elecom.2011.08.032

[20] S. Cherevko, X. Xing, C.-H. Chung, Hydrogen template assisted electrodeposition of sub-micrometer wires composing honeycomb-like porous Pb films, *Appl Surf Sci* **257** (2011) 8054–8061. doi:10.1016/j.apsusc.2011.04.098

[21] C.A. Marozzi, A.C. Chialvo, Development of electrode morphologies of interest in electrocatalysis. Part 1: Electrodeposited porous nickel electrodes, *Electrochim Acta* **45** (2000) 2111–2120. doi:10.1016/s0013-4686(99)00422-3

[22] X. Yu, M. Wang, Z. Wang, X. Gong, Z. Guo, The structure evolution mechanism of electrodeposited porous Ni films on NH_4Cl concentration, *Appl Surf Sci* **360** (2016) 502–509. doi: 10.1016/j.apsusc.2015.10.174

[23] S. Sengupta, A. Patra, S. Jena, K. Das, S. Das, A Study on the Effect of Electrodeposition Parameters on the Morphology of Porous Nickel Electrodeposits, *Metall Mater Trans A* **49** (2018) 920–937. doi:10.1007/s11661-017-4452-8

[24] S. Cherevko, N. Kulyk, C.-H. Chung, Nanoporous palladium with sub-10 nm dendrites by electrodeposition for ethanol and ethylene glycol oxidation, *Nanoscale* **4** (2012) 103–105. doi: 10.1039/c1nr11316j

[25] D. K. Oppedisano, L. A. Jones, T. Junk, S. K. Bhargava, Ruthenium electrodeposition from aqueous solution at high cathodic overpotential, *J Electrochem Soc* **161** (2014) D489–D494. doi:10.1149/2.0441410jes

[26] D. K. Zhuo, M.-G. Jeong, C.-H. Chung, Highly porous dendritic Ni–Sn anodes for lithium-ion batteries, *J Power Sources* **244** (2013) 601–605. doi:10.1016/j.jpowsour.2013.01.055

[27] L. Mattarozzi, S. Cattarin, N. Comisso, R. Gerbasi, P. Guerriero, M. Musiani, L. Vázquez-Gómez, E. Verlato, Electrodeposition of Cu-Ni alloy electrodes with bimodal porosity and their use for nitrate reduction, *ECS Electrochem Lett* **2** (2013) D58–D60. doi:10.1149/2.004311eel

[28] S. Eugenio, T. M. Silva, M. J. Carmezim, R. G. Duarte, M. F. Montemo, Electrodeposition and characterization of nickel–copper metallic foams for application as electrodes for supercapacitors, *J App Chem* **44** (2014) 455–465. doi:10.1007/s10800-013-0646-y

[29] L. D. Rafailovic, D. M. Minic, H. P. Karnthaler, J. Wosik, T. Trisovic, G. E. Nauer, Study of the dendritic growth of Ni–Co alloys electrodeposited on Cu substrates, *J Electrochem Soc* **157** (2010) D295–D301. doi:10.1149/1.3336957

[30] I. Najdovski, P.R. Selvakannan, A. P. O'Mullane, S. K. Bhargava, Rapid synthesis of porous honeycomb Cu/Pd through a hydrogen bubble templating method, *Chem Eur J* **17** (2011) 10058–10063. doi:10.1002/chem.201101224

[31] I. Najdovski, P.R. Selvakannan, S. K. Bhargava, A. P. O'Mullane, Formation of nanostructured porous Cu–Au surfaces: the influence of cationic sites on (electro)-catalysis, *Nanoscale* **4** (2012) 6298–6306. doi: 10.1039/c2nr31409f

[32] I. Najdovski, P.R. Selvakannana, A P. O'Mullane, Electrochemical formation of Cu/Ag surfaces and their applicability as heterogeneous catalysts, *RSC Adv*. **4** (2014) 7207–7215. doi: 10.1039/c3ra47557c

[33] S. Cherevko, N. Kulyka, C.-H. Chung, Pulse-reverse electrodeposition for mesoporous metal films: combination of hydrogen evolution assisted deposition and electrochemical dealloying, *Nanoscale* **4** (2012) 568–575. doi: 10.1039/c1nr11503k

[34] G.A. Lange, S. Eugénio, R.G. Duarte, T.M. Silva, M.J. Carmezim, M.F. Montemor, Characterisation and electrochemical behaviour of electrodeposited Cu–Fe foams applied as pseudocapacitor electrodes, *J Electroanal Chem* **737** (2015) 85–92. doi:10.1016/j.jelechem.2014.10.025

[35] J. Liu, L. Cao, W. Huang, Z. Li, Preparation of AuPt alloy foam films and their superior electrocatalytic activity for the oxidation of formic acid, *ACS Appl Mater Interfaces* **3** (2011) 3552–3558. doi:10.1021/am200782x

[36] X. Niu, H. Zhao, C. Chen, M. Lan, Enhancing the electrocatalytic activity of Pt–Pd catalysts by introducing porous architectures, *Chem Cat Chem* **5** (2013) 1416–1425. doi: 10.1002/cctc.201200658

[37] R. Li, H. Mao, J. Zhang, T. Huang, A. Yu, Rapid synthesis of porous Pd and PdNi catalysts using hydrogen bubble dynamic template and their enhanced catalytic performance for methanol electrooxidation, *J Power Sources* **24** (2013) 660–667. doi:10.1016/j.jpowsour.2013.05.032

[38] M. Jin, H. Ma, Electrochemical reductive dechlorination of trichloroacetic acid on porous Ag-Pd thin foam, *Russ J Electrochem* **49** (2013) 1081–1085. doi:10.1134/s1023193513110153

[39] L.D. Rafailović, C. Gammer, C. Rentenberger, T. Trišović, C. Kleber, H. P. Karnthaler, Enhanced oxygen evolution and reduction reactions of porous ternary NiCoFe foam electrodes prepared by dynamic hydrogen template deposition, *Nano Energy* **2** (2013) 523–529. doi:10.1016/j.nanoen.2012.12.004

[40] N.D. Nikolić, Lj.J. Pavlović, M.G. Pavlović, K.I. Popov, Formation of dish-like holes and a channel structure in electrodeposition of copper under hydrogen co-deposition, *Electrochim Acta* **52** (2007) 8096–8104. doi:10.1016/j.electacta.2007.07.008

[41] N.D. Nikolić, K.I. Popov, Lj. J. Pavlović, M.G. Pavlović, Phenomenology of a formation of a honeycomb – like structure during copper electrodeposition, *J Solid State Electrochem* **11** (2007) 667–675. doi: 10.1007/s10008-006-0222-z

[42] I. Najdovski, A. P. O'Mullane, The Effect of Electrode Material on the Electrochemical Formation of Porous Copper Surfaces using Hydrogen Bubble Templating, *J Electroanal Chem* **722-723** (2014) 95–101. doi:10.1016/j.jelechem.2014.03.034

[43] J.-H. Kim, R.-H. Kim, K. H-Sang, Preparation of copper foam with 3-dimensionally interconnected spherical pore network by electrodeposition, *Electrochem Commun* **10** (2008) 1148–1151. doi:10.1016/j.elecom.2008.05.035

[44] N.D. Nikolić, G. Branković, M.G. Pavlović, K.I. Popov, The effects of the pause to pulse ratio in the regime of pulsating overpotential on the formation of honeycomb-like structures, *Electrochem Commun* **11** (2009) 421–424. doi:10.1016/j.elecom.2008.12.007

[45] N.D. Nikolić, G. Branković, V.M. Maksimović, M.G. Pavlović, K.I. Popov, Influence of potential pulse conditions on the formation of honeycomb-like copper electrodes, *J Electroanal Chem* **635** (2009) 111–119. doi:10.1016/j.jelechem.2009.08.005

[46] N.D. Nikolić, G. Branković, V.M. Maksimović, M.G. Pavlović, K.I. Popov, Application of pulsating overpotential regime on the formation of copper deposits in the range of hydrogen co-deposition, *J Solid State Electrochem* **14** (2010) 331–338. doi:10.1007/s10008-009-0842-1

[47] N.D. Nikolić, G. Branković, Effect of parameters of square-wave pulsating current on copper electrodeposition in the hydrogen co-deposition range, *Electrochem Commun* **12** (2010) 740–744. doi:10.1016/j.elecom.2010.03.021

[48] N.D. Nikolić, G. Branković, V.M. Maksimović, Morphology and internal structure of copper deposits electrodeposited by the pulsating current regime in the hydrogen co-deposition range, *J Solid State Electrochem* **16** (2012) 321–328. doi:10.1007/s10008-011-1331-x

[49] N.D. Nikolić, G. Branković, K.I. Popov, Optimization of electrolytic process of formation of open and porous copper electrodes by the pulsating current (PC) regime, *Mater Chem Phys* **125** (2011) 587–594. doi:10.1016/j.matchemphys.2010.10.013

[50] N.D. Nikolić, G. Branković, Comparison of open porous copper structures obtained by the different current regimes of electrolysis, *Mater Lett* **70** (2012) 11–15. doi:10.1016/j.matlet.2011.11.081

[51] N.D. Nikolić, G. Branković, V.M. Maksimović, Effect of the anodic current density on copper electrodeposition in the hydrogen co-deposition range by the reversing current (RC) regime, *J Electroanal Chem* **661** (2011) 309–316. doi:10.1016/j.jelechem.2011.08.006

[52] M.S. Chandrasekar, M. Pushpavanam, Pulse and pulse reverse plating—Conceptual, advantages and applications, *Electrochim Acta* **53** (2008) 3313–3322. doi:10.1016/j.electacta.2007.11.054

[53] J.L. Barton, J.O'M. Bockris, The electrolytic growth of dendrites from ionic solutions, *Proc Roy Soc* **A268** (1962) 485–505. doi:10.1098/rspa.1962.0154.
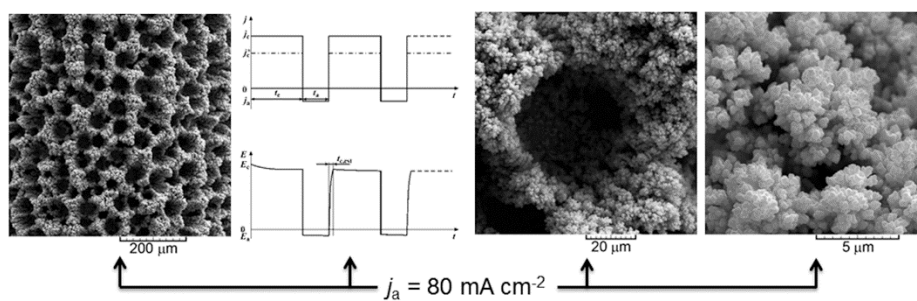
Cu deposits obtained in the hydrogen co-deposition range by the reversing current (RC) in the second range (j_c = 320 mA cm^{-2}; t_c = 10 s; t_a = 5 s)
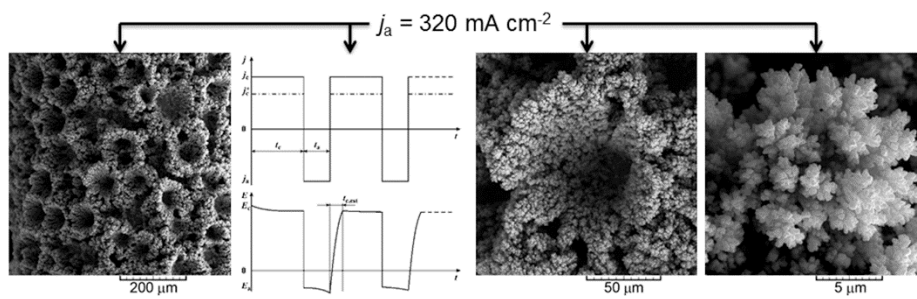
Graphical abstract

Research highlights

- Cu was electrodeposited by the reversing current (RC) regime in the hydrogen co-deposition range.
- The effect of the anodic current density on morphology of Cu deposits was examined.
- Comparison with the Cu deposit obtained in constant galvanostatic regime was made.
- The honeycomb-like structures were formed with the smaller anodic current densities.
- The non-uniform deposits with dendrites were formed with the larger anodic current densities.